
Article:
Çalik-Karaköse, U.H. and Askes, H. (2015) A recovery-type a posteriori error estimator for gradient elasticity. Computers and Structures, 154. 204 - 209. ISSN 0045-7949

https://doi.org/10.1016/j.compstruc.2015.04.003

A RECOVERY-TYPE A POSTERIORI ERROR ESTIMATOR FOR GRADIENT ELASTICITY

***Ülkü H. Çalık-Karaköse[1] and Harm Askes[2]**

[1]Faculty of Civil Engineering, Istanbul Technical University, Maslak, Istanbul, 34469, Turkey

[2]Department of Civil and Structural Engineering, University of Sheffield, Mappin Street, Sheffield, S1 3JD, United Kingdom

Key Words: Gradient elasticity; a posteriori error estimation; recovery-type error estimator

ABSTRACT

In this paper, an a posteriori error estimator of the recovery type is developed for the gradient elasticity theory of Aifantis. This version of gradient elasticity can be implemented in a staggered way, whereby solution of the classical equations of elasticity is followed by solving a reaction-diffusion equation that introduces the gradient enrichment and removes the singularities. With gradient elasticity, singularities in the stress field can be avoided, which simplifies error estimation. Thus, we develop an error estimator associated with the second step of the staggered algorithm. Stress-gradients are recovered based on the methodology of Zienkiewicz and Zhu, after which a suitable energy norm is discussed. The approach is illustrated with a number of examples that demonstrate its effectiveness.

*Corresponding author. Tel: +90 532 240 91 96.
E-mail addresses: calikkarakose@itu.edu.tr (Ülkü H. Çalık-Karaköse), h.askes@sheffield.ac.uk (Harm Askes)

1 INTRODUCTION

In classical elasticity, the stresses depend only on the first order derivative of displacements (strains) and not on higher-order derivatives. No information on the material's microstructure is present in classical elasticity, and as a consequence size-dependent behaviour cannot be captured with classical elasticity. Moreover, classical elasticity is plagued by the occurrence of singular stresses and strains at the tips of sharp cracks, re-entrant corners or where point loads are applied. An alternative to classical elasticity is so-called gradient elasticity, in which the field equations are equipped with additional higher-order spatial derivatives of the relevant state variables. The higher-order terms are accompanied by an additional material parameter with the dimensions of length – this parameter is linked to the micro-structural geometry and is called "internal length scale". Due to the presence of such an internal length scale, size-dependent mechanical behaviour can be described [5, 7]. Furthermore, the occurrence of singularities in the stress and strain field can be avoided with gradient elasticity.

One of the most versatile variants of gradient elasticity theory is the Aifantis theory [1-3]. Its attractiveness is due to its mathematical structure, which allows the fourth-order equilibrium equations to be solved as an uncoupled sequence of two sets of second-order equations [3]. For numerical implementations, this has the significant consequences that simple, C^0-continuous interpolations suffice for the spatial discretisation. This makes finite element implementation straightforward, as has been demonstrated in a number of studies [4-8].

We can use a priori and a posteriori error estimation techniques in order to determine the accuracy of numerical solutions. A systematic comparative presentation of these techniques is given in [9], and an in-depth discussion on various types of estimators can be obtained in [18]. The two main families of a posteriori error estimators are the residual type estimators [10,11] and the recovery type estimators [12-14] – here, the discussion will focus on the latter. The recovery type error estimators have been first introduced by Zienkiewicz and Zhu [12] and later, the authors presented the so-called superconvergent patch recovery method which improved the performance of recovery based methods [13,14]. This error estimate can also be applied to hierarchical p-refinement with a slight modification as given in [15]. A local a posteriori error estimator for the extended finite element method is devised in [16] which is based on a derivative recovery technique in the L_2 norm and is applied to linear elastic fracture mechanics. In their later study, the authors proposed an extended global derivative recovery technique for extended finite elements [17].

Thus, recovery type error estimators can be devised for use in fracture mechanics, where singularities are known to exist in the solution. However, and as argued above, it is also possible to analyse cracks with gradient elasticity by which singularities in the stress field can be avoided altogether. This should facilitate error estimation, and in this study a recovery type a posteriori error estimator for gradient elasticity will be developed. After revisiting the basic equations of the Aifantis gradient elasticity theory in Section 2 and its finite element implementation in Section 3, the suggested error estimator will be discussed in Section 4. The effectiveness of this approach is demonstrated with two benchmark problems in Section 5.

2 AIFANTIS' GRADIENT ELASTICITY THEORY

One of the most popular gradient elasticity theories is the one derived by Aifantis and co-workers in the early 1990s [1-3]. In this theory, the usual linear elastic constitutive relations are extended with the Laplacian of the strain as

$$\sigma_{ij} = C_{ijkl}\left(\varepsilon_{kl} - \ell^2 \varepsilon_{kl,mm}\right) \tag{1}$$

where σ is the Cauchy stress, C is the constitutive tensor, ε is the usual infinitesimal strain and ℓ is an internal length scale parameter representing the microstructure of the material. The equilibrium equations can be written in terms of displacement derivatives as

$$C_{ijkl}\left(u_{k,jl} - \ell^2 u_{k,jlmm}\right) + b_i = 0 \tag{2}$$

where b are the body forces. The attractiveness of this theory is (i) that it contains only one internal length scale parameter, and (ii) that its mathematical structure allows to solve the fourth-order partial differential equations as an uncoupled sequence of two sets of second-order equations. More specifically, the various derivatives in Eq. (2) can be factorised, so that Eq. (2) can be rewritten as

$$C_{ijkl} u^{c}_{k,\,jl} + b_i = 0 \tag{3}$$

which are the equations of classical elasticity, followed by

$$u^{g}_{k} - \ell^2 u^{g}_{k,mm} = u^{c}_{k} \tag{4}$$

Here u^c are the displacements following from the classical elasticity equations, whilst u^g are the gradient-enriched displacements. Note that u^g in Eq. (4) is identical to u in Eq. (2), and the superscript g is used to distinguish the gradient-enriched displacements from its classical counterpart.

If Eq. (4) is substituted back into Eq. (3), it is easily verified that Eq. (2) is retrieved. When this operator split was suggested first by Ru and Aifantis [3], the gradient enrichment was expressed in terms of displacements as given in Eq. (4). However, it can also be evaluated in terms of stresses by differentiation as

$$\sigma^{g}_{ij} - \ell^2 \sigma^{g}_{ij,mm} = C_{ijkl} u^{c}_{k,l} \tag{5}$$

The use of Eq. (5) instead of Eq. (4) has some advantages: it was demonstrated in [5,6] that the use of Eq. (4) does not necessarily remove the singularities from all stress components at the tip of sharp cracks, whereas all stress singularities are removed if Eq. (5) is used – this discrepancy can be attributed to the nature of the variationally consistent boundary conditions [5].

3 IMPLEMENTATION OF AIFANTIS' THEORY

In this section, matrix-vector notation will be used instead of index notation, as is customary in finite element literature. A finite element implementation of the Aifantis' theory which is based on Eq. (4) was first given in [4] and then extended to include Eq. (5) in [5]. In this study, and following the recommendations in [5], Eqns. (3) and (5) are used for the implementation of the Aifantis theory of gradient elasticity.

Eq. (3) is the usual expression of equilibrium in classical elasticity, the spatial discretisation of which is well known and does not need to be repeated here. The weak form of Eq. (5) is obtained by premultiplying with a virtual strain field $\delta\mathbf{e}$ and integrating over the domain Ω as

$$\int_{\Omega} \delta\mathbf{e}^{\mathrm{T}} \cdot (\boldsymbol{\sigma} - \ell^2 \nabla^2 \boldsymbol{\sigma} - \mathbf{C}\mathbf{L}\mathbf{u}) \mathrm{dV} = 0 \tag{6}$$

where L is the usual strain-displacement differential operator, which in the two dimensional case is defined as

$$\mathbf{L}^{\mathrm{T}} = \begin{bmatrix} \dfrac{\partial}{\partial \mathrm{x}} & 0 & \dfrac{\partial}{\partial \mathrm{y}} \\ 0 & \dfrac{\partial}{\partial \mathrm{y}} & \dfrac{\partial}{\partial \mathrm{x}} \end{bmatrix} \tag{7}$$

Integrating by parts and substituting $\delta\mathbf{e} = \mathbf{S}\delta\boldsymbol{\sigma}$, where $\mathbf{S} = \mathbf{C}^{-1}$, results in

$$\int_{\Omega} \delta\boldsymbol{\sigma}^{\mathrm{T}} \mathbf{S} \boldsymbol{\sigma} \mathrm{dV} + \int_{\Omega} \left(\frac{\partial \boldsymbol{\sigma}^{\mathrm{T}}}{\partial \mathrm{x}} \mathrm{Sl}^2 \frac{\partial \boldsymbol{\sigma}}{\partial \mathrm{x}} + \frac{\partial \boldsymbol{\sigma}^{\mathrm{T}}}{\partial \mathrm{y}} \mathrm{Sl}^2 \frac{\partial \boldsymbol{\sigma}}{\partial \mathrm{y}} \right) \mathrm{dV} - \int_{\Omega} \delta\boldsymbol{\sigma}^{\mathrm{T}} \mathbf{L}\mathbf{u} \mathrm{dV} = 0 \tag{8}$$

Here, the boundary terms are ignored, which is equivalent to adopting the homogeneous natural boundary condition $\mathbf{n} \cdot \nabla \boldsymbol{\sigma} = 0$ [5, 7]. Finite element discretisation of Eq. (8) gives

$$\underline{\delta\sigma}^{\mathrm{T}} \int_{\Omega} \left(\mathrm{N}_{\sigma}^{\mathrm{T}} \mathrm{S} \mathrm{N}_{\sigma} + \frac{\partial \mathrm{N}_{\sigma}^{\mathrm{T}}}{\partial \mathrm{x}} \mathrm{S} \ell^2 \frac{\partial \mathrm{N}_{\sigma}}{\partial \mathrm{x}} + \frac{\partial \mathrm{N}_{\sigma}^{\mathrm{T}}}{\partial \mathrm{y}} \mathrm{S} \ell^2 \frac{\partial \mathrm{N}_{\sigma}}{\partial \mathrm{y}} \right) \mathrm{dV} \underline{\sigma} = \underline{\delta\sigma}^{\mathrm{T}} \int_{\Omega} \mathrm{N}_{\sigma}^{\mathrm{T}} \mathrm{B}_{\mathrm{u}} \mathrm{dV} \underline{\mathrm{u}} \tag{9}$$

The two fields of unknowns, namely the classical displacements and the gradient-enriched stresses, are discretised with shape functions N_{u} and N_{σ}, respectively. Furthermore, $\mathrm{B}_{\mathrm{u}} = \mathrm{L}\mathrm{N}_{\mathrm{u}}$ and underlined vectors contain the discretised nodal values of their continuous counterparts. With these specifications, the resulting system of equations can be written as

$$\begin{bmatrix} \mathrm{K}_{\mathrm{uu}} & 0 \\ -\mathrm{K}_{\mathrm{u}\sigma}^{\mathrm{T}} & \mathrm{K}_{\sigma\sigma} \end{bmatrix} \begin{bmatrix} \underline{\mathrm{u}} \\ \underline{\sigma} \end{bmatrix} = \begin{bmatrix} \underline{\mathrm{f}} \\ \underline{0} \end{bmatrix} \tag{10}$$

where $\underline{\mathrm{f}}$ is the external force vector, and

$$\mathrm{K}_{\mathrm{uu}} = \int \mathrm{B}_{\mathrm{u}}^{\mathrm{T}} \mathrm{C} \mathrm{B}_{\mathrm{u}} \mathrm{dV} \tag{11}$$

$$\mathrm{K}_{\mathrm{u}\sigma} = \int \mathrm{B}_{\mathrm{u}}^{\mathrm{T}} \mathrm{N}_{\sigma} \mathrm{dV} \tag{12}$$

$$\mathrm{K}_{\sigma\sigma} = \int \left(\mathrm{N}_{\sigma}^{\mathrm{T}} \mathrm{S} \mathrm{N}_{\sigma} + \frac{\partial \mathrm{N}_{\sigma}^{\mathrm{T}}}{\partial \mathrm{x}} \mathrm{S} \ell^2 \frac{\partial \mathrm{N}_{\sigma}}{\partial \mathrm{x}} + \frac{\partial \mathrm{N}_{\sigma}^{\mathrm{T}}}{\partial \mathrm{y}} \mathrm{S} \ell^2 \frac{\partial \mathrm{N}_{\sigma}}{\partial \mathrm{y}} \right) \mathrm{dV} \tag{13}$$

Eq. (10) is a decoupled system of equations in which the first row of equations can be solved prior to the second row of equations. Thus, it can be said that the gradient-enrichment (second row of equations) constitutes a post-processing of the results of classical elasticity (first row of equations).

4 RECOVERY TYPE ERROR ESTIMATION FOR GRADIENT ELASTICITY

Next, one of the a posteriori error estimates derived by Zienkiewicz and Zhu [12] is adapted to the finite element implementation of gradient elasticity. In their study, a nodal averaging method is used to recover the stresses as an approximation of the exact stresses which are in general unknown. These recovered stresses are much more accurate than the direct finite element solution, and therefore the difference between recovered stresses and finite element stresses is a good approximation of the actual error in the stresses. The error in the stresses is accordingly defined as

$$\mathrm{e}_{\sigma} = \sigma_{\mathrm{n}} - \sigma_{\mathrm{r}} \tag{14}$$

where the subscripts n and r indicate “numerical” and “recovered”, respectively.

The error defined in Eq. (14) can be used to estimate the error in particular locations of the domain. However, as a first indication of the overall error of a certain finite element computation, it is common to compute the error field across the entire domain in a suitably defined norm. If so desired, this can afterwards be used to normalise local errors such as those used in adaptive h-refinement algorithms, e.g. Following Zienkiewicz and Zhu, we will adopt an energy norm. From the continuum equations (3) and (5) it can be seen that the underlying energy functionals are

$$\mathrm{U}_1 = \int_{\Omega} \frac{1}{2} \varepsilon_{\mathrm{ij}}^{\mathrm{c}} \mathrm{C}_{\mathrm{ijkl}} \varepsilon_{\mathrm{kl}}^{\mathrm{c}} \mathrm{dV} - \int_{\Omega} \mathrm{u}_{\mathrm{i}}^{\mathrm{c}} \mathrm{b}_{\mathrm{i}} \mathrm{dV} - \int_{\Gamma} \mathrm{u}_{\mathrm{i}}^{\mathrm{c}} \mathrm{t}_{\mathrm{i}} \mathrm{dS} \tag{15}$$

associated with Eq. (3), and

$$\mathrm{U}_2 = \int_{\Omega} \frac{1}{2} \left(\sigma_{\mathrm{ij}} \mathrm{S}_{\mathrm{ijkl}} \sigma_{\mathrm{kl}} + \ell^2 \sigma_{\mathrm{ij,m}} \mathrm{S}_{\mathrm{ijkl}} \sigma_{\mathrm{kl,m}} \right) \mathrm{dV} - \int_{\Omega} \sigma_{\mathrm{ij}} \varepsilon_{\mathrm{ij}}^{\mathrm{c}} \mathrm{dV} \tag{16}$$

corresponding to Eq. (5). The last term in Eq. (16) provides the coupling from Eq. (3) to Eq. (5) and can be interpreted as “source term” for Eq. (5). Based on Eq. (16), an energy norm of the error associated with Eq. (5) can be defined as

$$\|e_\sigma\|^2 = \int_\Omega \frac{1}{2}\left\{(\sigma_n - \sigma_r)^T S(\sigma_n - \sigma_r) + \ell^2 (\nabla\sigma_n - \nabla\sigma_r)^T S(\nabla\sigma_n - \nabla\sigma_r)\right\} dV \quad (17)$$

Here, $\nabla\sigma_n$ is the stress gradient vector of the numerical solution and $\nabla\sigma_r$ is the recovered stress gradient vector. However, since the stresses are the primary variables in Eq. (5), it follows that $\sigma_n \equiv \sigma_r$ so that the first contribution in the integral of Eq. (17) vanishes identically. Eq. (17) can therefore be simplified as

$$\|e_\sigma\|^2 = \int_\Omega \frac{1}{2}\ell^2 (\nabla\sigma_n - \nabla\sigma_r)^T S(\nabla\sigma_n - \nabla\sigma_r) dV \quad (18)$$

Thus, the energy norm of the error is expressed in terms of the derivatives of the primary variables, as usual. We will also employ a relative error η defined by

$$\eta = \frac{\|e_\sigma\|}{\|\sigma\|} \quad (19)$$

Finally, the energy norm of the exact error is measured by

$$\|e_\sigma\|^2_{exact} = \int_\Omega \frac{1}{2}\ell^2 (\nabla\sigma_n - \nabla\sigma_{exact})^T S(\nabla\sigma_n - \nabla\sigma_{exact}) dV \quad (20)$$

Thus, the global error effectivity index is defined as the ratio of the approximate error to the exact error

$$\theta = \frac{\|e_\sigma\|}{\|e_\sigma\|_{exact}} \quad (21)$$

5 BENCHMARK EXAMPLES

5.1 Cantilever Beam

A plane stress cantilever beam example subjected to a unit point load shown in Figure 1 is solved by classical and gradient elasticity theories for coarse and successively refined meshes and the three stress components under the point load are given in Table 1 where $\boldsymbol{\sigma}^c$ and $\boldsymbol{\sigma}^g$ indicate stresses obtained from classical and gradient elasticity solutions, respectively.

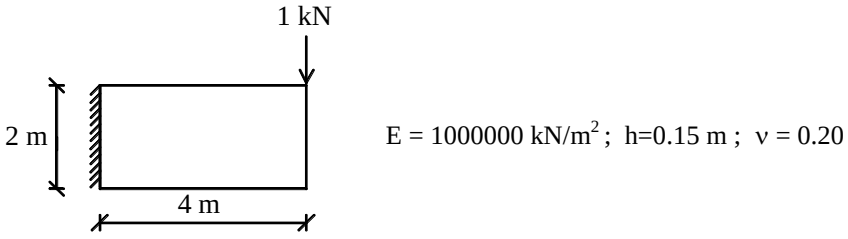

Figure 1 Cantilever beam under a tip load of 1kN

Table 1 Mesh refinement study for stresses under the point load

Mesh	σ^c_{xx}	σ^g_{xx}	σ^c_{yy}	σ^g_{yy}	σ^c_{xy}	σ^g_{xy}
(2x1)	4.150	3.131	-5.233	-3.846	-2.774	-3.047
(4x2)	4.901	2.997	-19.966	-8.740	-4.147	-3.736
(8x4)	8.625	3.037	-40.610	-10.431	-9.879	-4.280
(16x8)	17.593	3.131	-80.867	-11.186	-20.716	-4.537
(32x16)	35.373	3.193	-161.550	-11.571	-41.745	-4.645

The three stress components of classical elasticity solution roughly double in value for every successive mesh refinement corresponding to divergence. On the contrary, stress components converge to finite values when gradient elasticity is used.

Stresses along the cantilever beam obtained by classical elasticity and Aifantis' gradient elasticity theories for 5 different meshes are shown in Figures 2 and 3, respectively. In classical elasticity solution, the singularities under the point load cannot be captured for very coarse meshes but with mesh refinement, those singularities become apparent, as expected. In Figure 3, it is shown that singularities are eliminated by the usage of gradient elasticity.

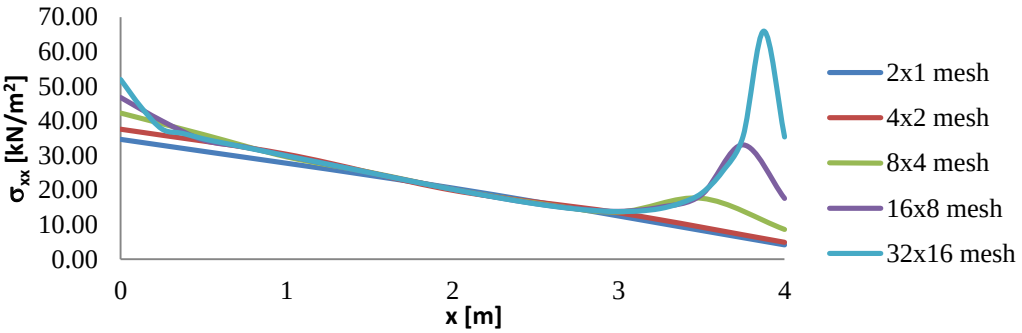

Figure 2 Mesh refinement study of classical elasticity solution

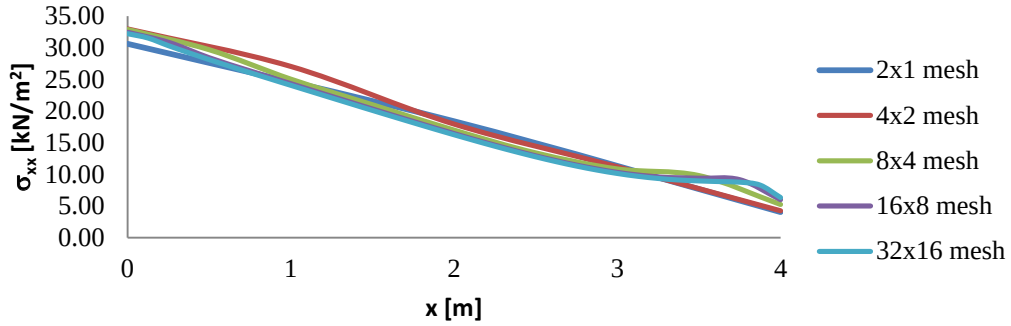

Figure 3 Mesh refinement study of gradient elasticity solution

Relative errors in stresses obtained for h refinement using different length scale parameters in log-log scale are plotted in Figure 4 to examine the convergence of the implementation. It is seen that relative errors decrease considerably with the increment of number of degrees of freedom (DOF). Furthermore, the convergence rate is somewhat higher for larger values of the length scale, which can be explained by the stress smoothing resulting from the gradient enrichment. Thus, the stress field is smoother, and convergence is easier to achieve, for larger values of the length scale.

In Figure 5, relative errors for increasing length scale parameters are shown for 4 different meshes. The convergence rate increases with mesh refinement as expected, although the error reduction is different for different values of the length scale. In line with what can be seen in Figure 4, the error is somewhat larger for $\ell = 1$ m

The effectivity index of the estimator is plotted against mesh refinement in logarithmic scale for different length scale parameters in Figure 6. It is observed that the effectivity index is very close to 1 for all analyses. Furthermore, it converges to 1 with both mesh refinement and increasing length scale parameter, which demonstrates the effectiveness of the proposed error estimator.

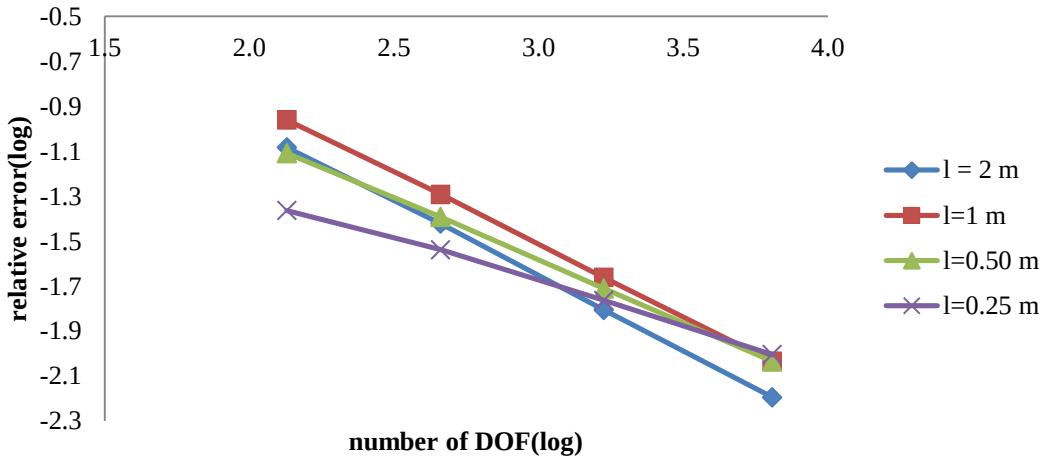

Figure 4 Relative errors in stresses for h refinement using different length scale parameters

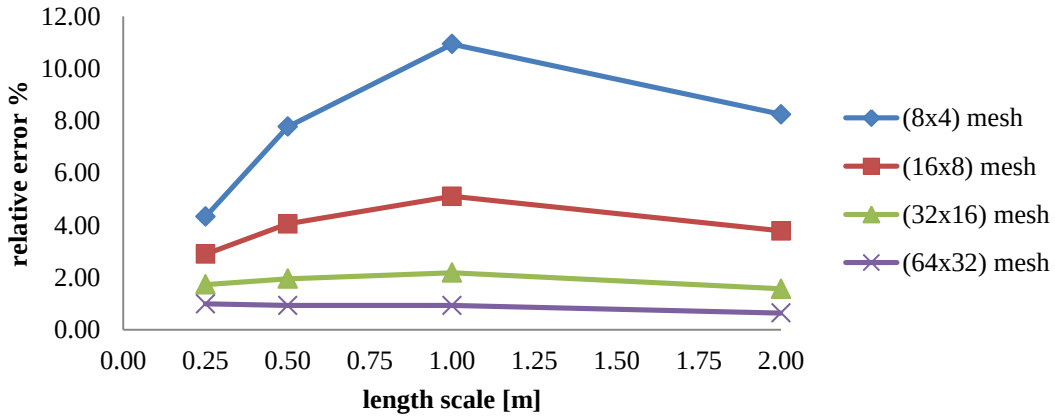

Figure 5 Relative errors in stresses for increasing length scale parameters

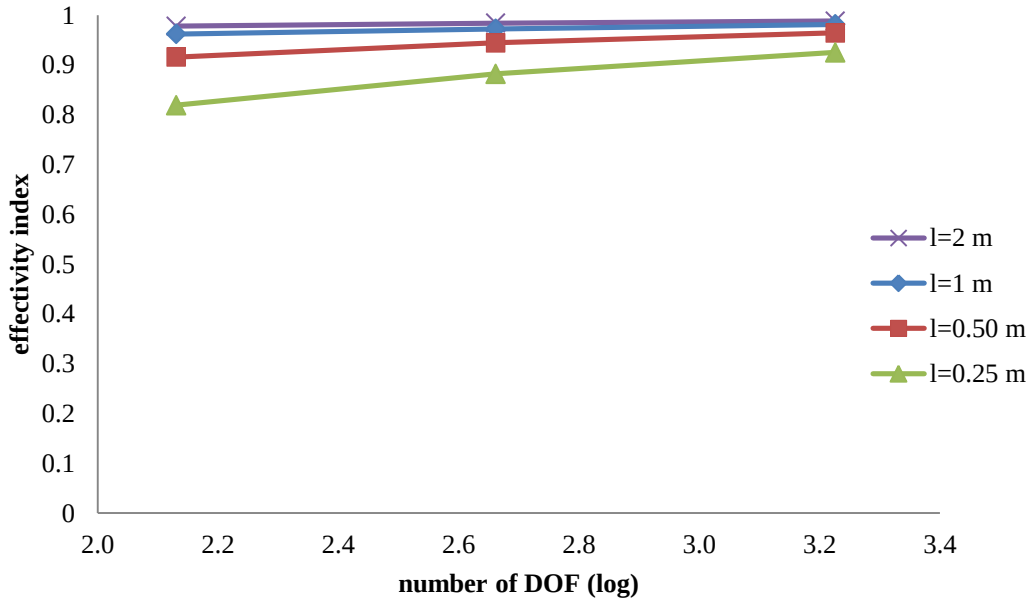

Figure 6 Effectivity index for h refinement and different length scale parameters

5.2 Tensile Strip Specimen

A plane stress tensile strip specimen made of polymethylmethacrylate (PMMA) shown in Figure 7 has two opposite crack-like U-notches of 6 mm in the middle and it is subjected to a uniformly distributed tensile force. Experimental study of the tensile strip specimen is given in [19] and its internal length scale parameter validation is performed in [20]. First, stress distributions along the midline are obtained both by classical and gradient elasticity theories for 3 successively refined meshes and for 4 length scale parameters. Afterwards, relative errors are examined for h refinement and for 4 length scale parameters. Finally, effectivity indexes are obtained in order to demonstrate the effectiveness of the proposed a posteriori error estimation approach.

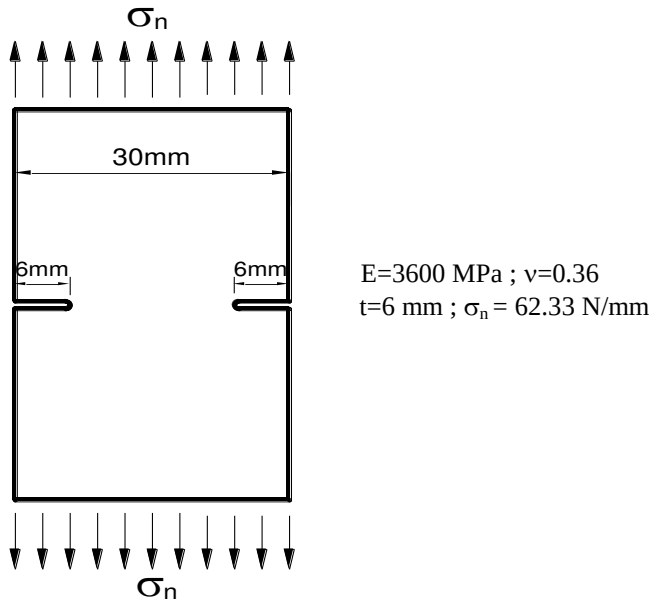

Figure 7 Geometry of the U-notched tensile strip specimen

Note that, due to its symmetry property, one quarter of the specimen is used for simplicity. In Figure 8, a coarse mesh of 15x15 elements is used and stresses in y direction are plotted against the distance. Stresses up to the crack tip are all about zero as expected and they attain unrealistic values around the crack tip when classical elasticity is used. It can be observed in Figures 8, 9, and 10 that those values are smoothed by the usage of gradient elasticity and more realistic values are obtained with the increment of the length scale parameter.

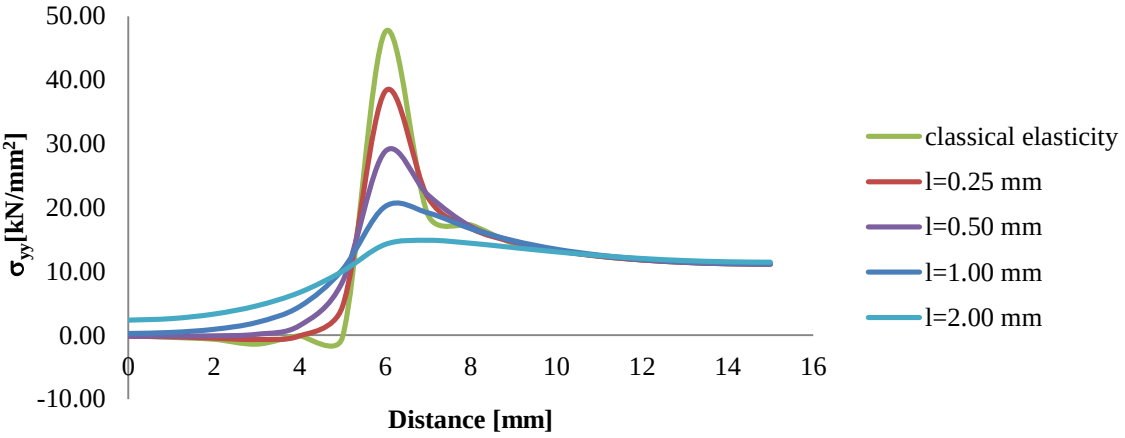

Figure 8 Stresses along the edge of the one quarter specimen using (15x15) mesh

The number of elements in both directions is doubled in Figure 8 and it is seen that there is a noticeable jump in stresses of classical elasticity around the crack tip. In Figure 9, the number of elements is increased again leading to a (60x60) mesh. The jump in stresses of classical elasticity solution increases which means that the singularities can be observed more clearly when small mesh sizes are used.

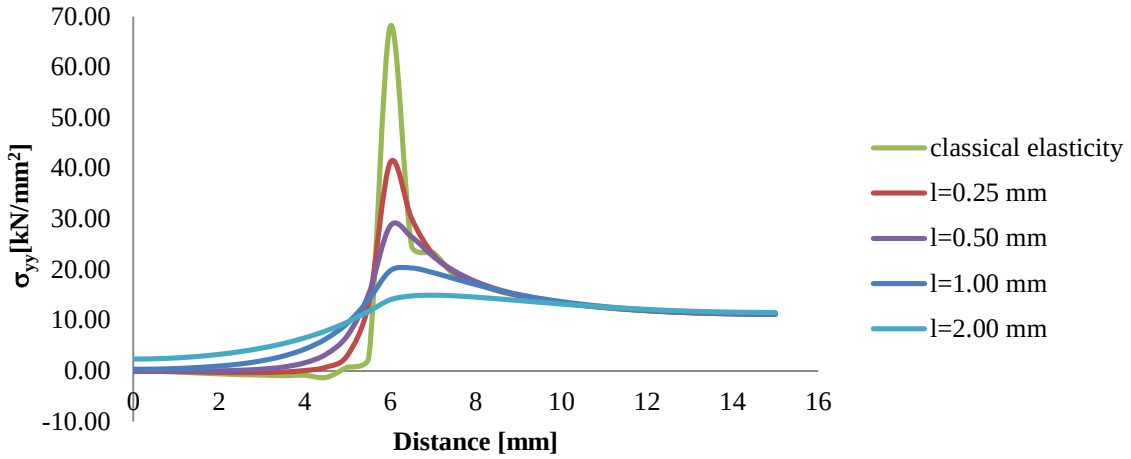

Figure 9 Stresses along the edge of the one quarter specimen using (30x30) mesh

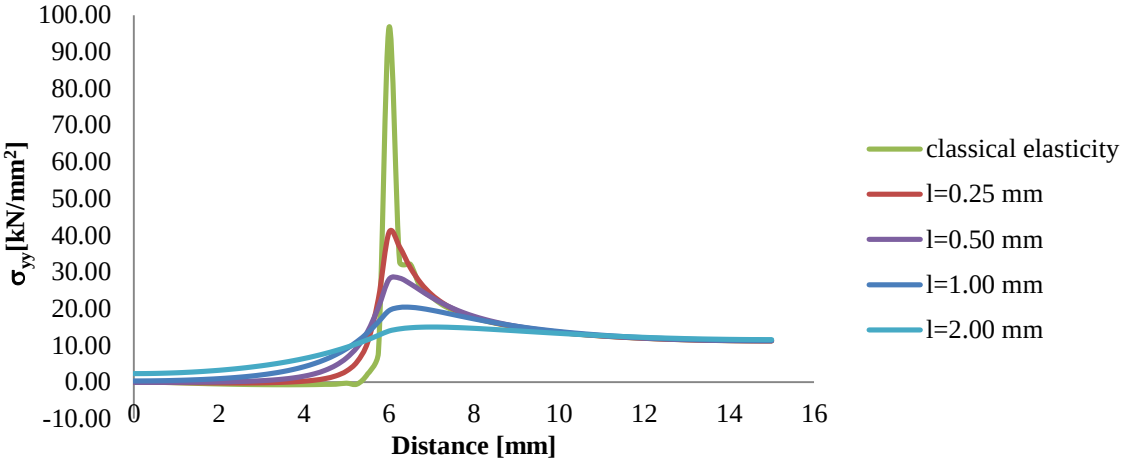

Figure 10 Stresses along the edge of the one quarter specimen using (60x60) mesh

In order to examine the convergence of the implementation, relative errors in stresses are obtained for h refinement using different length scale parameters as given in Figure 11, plotted in log-log scale. It is seen that relative errors decrease considerably with increasing the number of degrees of freedom as well as the length scale parameter. The length scale with a value of 0.25 mm is very small compared to the element sizes of the coarsest meshes, therefore the behaviour of the error is out of line with the other values of the length scale (although the error is still monotonically decreasing with the element size).

In Figure 12, relative errors for increasing length scale parameters are shown for 5 different meshes. As expected, the convergence rate increases with mesh refinement. However, another observation is that larger values of the length scale generally lead to lower levels of error. This is because larger values of the length scale lead to more smoothed-out stress distributions, which can be captured more easily by the finite element discretisation, thus leading to lower errors.

Finally, the effectivity index of the estimator is plotted against mesh refinement in logarithmic scale for different length scale parameters in Figure 13 and it is seen that the effectivity index is very close to 1 for all analyses. This demonstrates the effectiveness of the proposed error estimator.

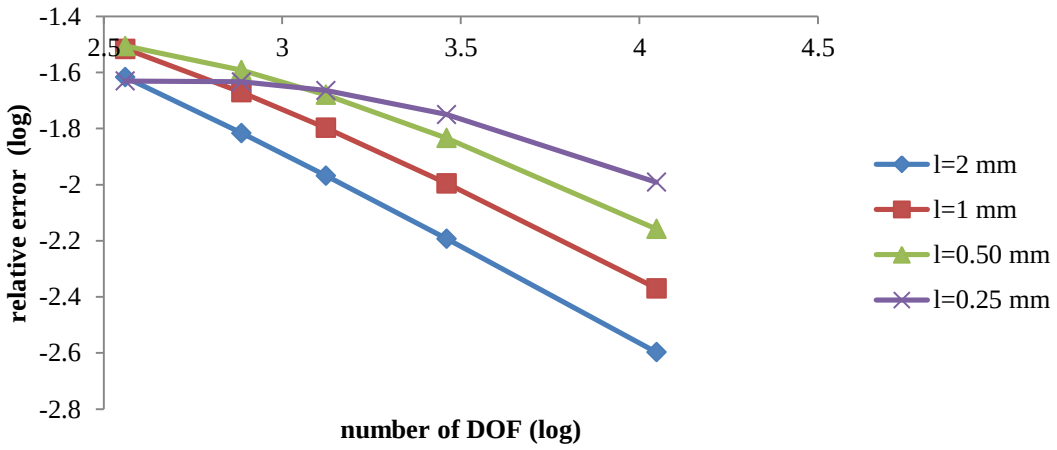

Figure 11 Relative errors in stresses for h refinement using different length scale parameters

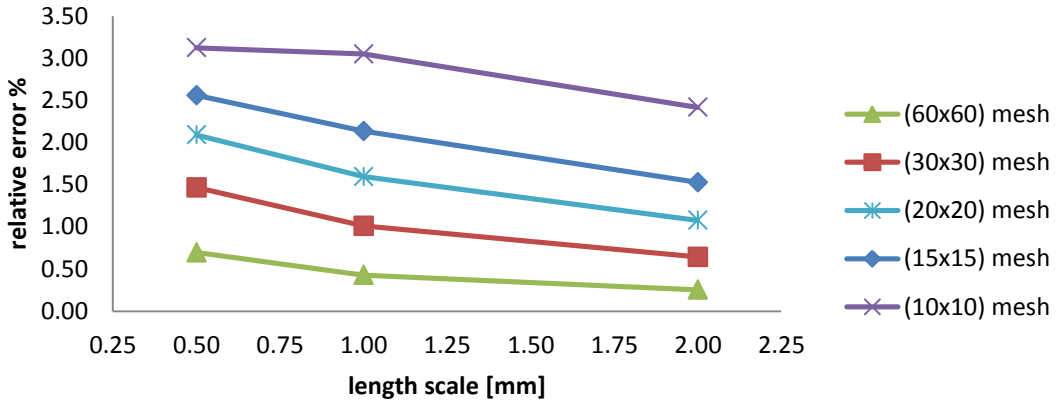

Figure 12 Relative errors in stresses for increasing length scale parameters

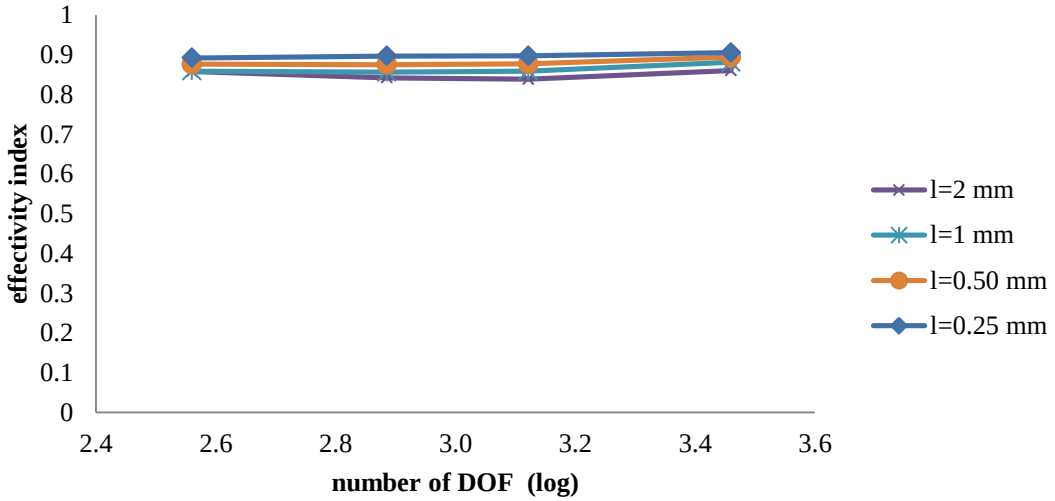

Figure 13 Effectivity index for h refinement and different length scale parameters

6 CONCLUSIONS

In this paper, a recovery type a posteriori error estimator is developed for the Aifantis' gradient elasticity theory. This version of gradient elasticity can be implemented in a staggered way whereby the fourth-order equilibrium equations are solved as an uncoupled sequence of two sets of second-order equations. Thus, simple, C^0-continuous interpolations suffice for the spatial discretisation which makes the finite element implementation straightforward. The developed error estimator is associated with the second step of the staggered algorithm where stress-gradients are recovered based on the methodology of Zienkiewicz and Zhu, after which a suitable energy norm is discussed.

It is demonstrated with two benchmark examples that stress singularities under point loads and around crack tips are avoided with gradient elasticity which simplifies error estimation. It is observed that the relative error decreases and the convergence rate increases with mesh refinement as well as, generally, with increasing length scale parameter.

In order to investigate the effectiveness of the proposed error estimator, the effectivity index is plotted against mesh refinement for different length scale parameters and it is seen that the effectivity index of the estimator is very close to 1 for all analyses which demonstrates that the proposed method is effective.

Finally, it is noted that in this paper we have used artificial values for the gradient elasticity length scale, solely to test the developed error estimator. In real-life applications, the value of the length scale should be measured from experiments or deduced from the micro-structural geometry of the materials – see [7] for an overview.

References

[1] Aifantis E.C. (1992). On the role of gradients in the localization of deformation and fracture. International Journal of Engineering Science 30, 1279-1299.

[2] Altan S.B. and Aifantis E.C. (1992). On the structure of the mode III crack-tip in gradient elasticity. Scripta Metallurgica et Materalia 26, 319-324.

[3] Ru C.Q. and Aifantis E.C. (1993). A simple approach to solve boundary-value problems in gradient elasticity. Acta Mechanica 101, 59-68.

[4] Tenek L.T. and Aifantis E.C. (2002). A two-dimensional finite element implementation of a special form of gradient elasticity. Computer Modeling in Engineering & Sciences 3, 731-741.

[5] Askes H., Morata I. and Aifantis E.C. (2008). Finite element analysis with staggered gradient elasticity. Computers and Structures, 86, 1266-1279.

[6] Askes H. and Gitman I. (2009). Non-singular stresses in gradient elasticity at bi-material interface with transverse crack. International Journal of Fracture, 156,217–222.

[7] Askes H. and Aifantis E.C. (2011). Gradient elasticity in statics and dynamics: An overview of formulations, length scale identification procedure, finite element implementations and new results. International Journal of Solids and Structures, 48, 1962-1990.

[8] Askes H. (2011). Gradient elasticity theories and finite element implementations for static fracture. Forni di Sopra (UD), Italy, March 7-9, 136-142.

[9] Stewart J.R. and Hughes T.J.R. (1998). A tutorial in elementary finite element error analysis: A systematic presentation of a priori and a posteriori error estimates. Computer Methods in Applied Mechanics and Engineering, 158, 1-22.

[10] Babuška I, Rheinboldt C (1978). A-posteriori error estimates for the finite element method. International Journal for Numerical Methods in Engineering, 12, 1597–1615.

[11] Díez P, Egozcue JJ, Huerta A (1998) A posteriori error estimation for standard finite element analysis. Computer Methods in Applied Mechanics and Engineering, 163, 141–157.

[12] Zienkiewicz O.C., Zhu J.Z. (1987). A simple error estimator and adaptive procedure for practical engineering analysis. International Journal for Numerical Methods in Engineering, 24, 337-357.

[13] Zienkiewicz O.C., Zhu J.Z. (1992). The superconvergent patch recovery and a posteriori error estimates. Part 1: The recovery technique. International Journal for Numerical Methods in Engineering, 33 (77), 1331-1364.

[14] Zienkiewicz O.C., Zhu J.Z. (1992). The superconvergent patch recovery and a posteriori error estimates. Part 2: Error estimates and adaptivity. International Journal for Numerical Methods in Engineering, 33 (77), 1365-1382.

[15] Oh H-S., Batra R.C. (1999). Application of Zienkiewicz-Zhu's error estimate with superconvergent patch recovery to hierarchical p-refinement. Finite Elements in Analysis and Design, 31, 273-280.

[16] Bordas S., Duflot M. (2007). Derivative recovery and a posteriori error estimate for extended finite elements, Computer Methods in Applied Mechanics and Engineering, 196, 3381-3399.

[17] Duflot M., Bordas S. (2008). A posteriori error estimation for extended finite elements by an extended global recovery. International Journal for Numerical Methods in Engineering, 76, 1123–1138.

[18]Ainsworth M, Oden JT (2000). A posteriori error estimation in finite element analysis. Wiley, New York.

[19] Livieri P. (2008). Use of J-integral to predict static failures in sharp V-notches and rounded U-notches. Engineering Fracture Mechanics, 75, 1779-1793.

[20] Askes H., Çalık-Karaköse Ü.H. and Susmel L. (2012). Gradient Elasticity Length Scale Validation Using Static Fracture Experiments of PMMA and PVC. International Journal of Fracture, 176, 223–227.